Intravital Imaging of IL-1β Production in Skin

Hironori Matsushima[1,2], Yasushi Ogawa[2], Toru Miyazaki[3], Hiroaki Tanaka[2], Akiko Nishibu[2] and Akira Takashima[1,2]

IL-1 is a prototypic inflammatory cytokine that has pathogenic roles in various skin disorders. Although Langerhans cells (LCs) have been reported to express IL-1β mRNA upon application of contact sensitizers, it remains unclear whether other cell types produce IL-1β in skin. Thus, we sought to directly identify IL-1β-producing cells in living animals by construction of transgenic mice expressing DsRed fluorescence protein gene under the control of IL-1β promoter. Little DsRed fluorescence signal was detected in skin under steady-state conditions. Striking increases in DsRed signal were observed after topical application of a contact sensitizer, oxazolone, which also induced markedly elevated IL-1β mRNA and protein expression. DsRed signal was expressed primarily by $CD45^-/CD11b^+$ myeloid leukocytes in both epidermal and dermal compartments and was detected only in small fractions of epidermal LCs. Interestingly, $DsRed^-$ cells emerged preferentially as clusters around hair follicles. Intravital confocal imaging experiments revealed highly motile potentials of $DsRed^+$ cells—they constantly crawled around hair follicles via amoeba-like movements with a mean velocity of $1.0 \pm 0.4\,\mu m\,min^{-1}$ (epidermis) or $2.7 \pm 1.4\,\mu m\,min^{-1}$ (dermis). The newly developed *in vivo* imaging system represents a useful tool for studying spatial regulation of IL-1β production in skin.

Journal of Investigative Dermatology (2010) **130,** 1571–1580; doi:10.1038/jid.2010.11; published online 11 February 2010

INTRODUCTION

Cytokines of the IL-1 family function as potent mediators and regulators of host inflammatory responses to infection and tissue injury. Of the 11 members of this family, IL-1β is the best-studied cytokine, with diverse phenotypes reported for IL-1β-deficient mice (Dinarello, 2009). On exposure to pathological stimuli, IL-1β is produced by activated leukocytes such as neutrophils, monocytes, macrophages, and dendritic cells (DCs) (O'Neill, 2008), leading to induction and enhancement of inflammatory responses. Bioactive IL-1β (18 kDa) is generated by caspase-1-dependent cleavage of an inactive precursor (31 kDa), pro-IL-1β (Cerretti *et al.*, 1992; Thornberry *et al.*, 1992). Recent studies have revealed that the inflammasome, the intracellular caspase-1-activating complex, serves as a key intracellular compartment for processing and secretion of bioactive IL-1β (Dinarello, 2009; Martinon *et al.*, 2009). Under inflammatory conditions, activation of the P2X7 receptor with extracellular ATP triggers the assembly of inflammasome components, resulting in the formation of active caspase-1 from procaspase-1. It should be stated, however, that pro-IL-1β may be processed in a caspase-1-independent manner by several proteases, such as neutrophil proteinase-3, elastase, matrix metalloprotease 9, and granzyme A, illustrating highly complex regulatory mechanisms (Fantuzzi *et al.*, 1997; Coeshott *et al.*, 1999; Sugawara *et al.*, 2001).

As an outermost tissue, the skin is constantly exposed to a variety of environmental insults, such as harmful chemicals, physical stimuli, and infectious microbes. It is well known that IL-1 functions as a key regulator of local host responses to such pathological stimuli. As early as in the early 1980s, an IL-1-like activity, termed the "epidermal cell-derived thymocyte-activating factor," was found to be produced in the skin (Luger *et al.*, 1982; Kupper *et al.*, 1986; Kupper, 1990). Primary cultures and cell lines derived from keratinocytes and Langerhans cells (LCs) in the epidermis, as well as from fibroblasts, endothelial cells, and DCs in the dermis, have been reported to produce IL-1α and/or IL-1β upon *in vitro* exposure to various stimuli (Enk and Katz, 1992; Takashima and Bergstresser, 1996). With regard to biological activities of IL-1 in skin, IL-1β-deficient mice were reported to manifest impaired contact hypersensitivity responses to trinitrochlorobenzene, which was applied topically for sensitization and injected into the footpad for elicitation (Shornick *et al.*, 1996; Nakae *et al.*, 2001; Nambu *et al.*, 2006). In a standard contact hypersensitivity model (in which trinitrochlorobenzene was applied topically for both sensitization and elicitation), however, reduced ear swelling responses were observed in IL-1α-deficient mice, but not in IL-1β-deficient mice (Shornick *et al.*, 1996; Nakae *et al.*, 2001; Nambu *et al.*, 2006). Conversely, the same group subsequently reported

[1]*Department of Medical Microbiology and Immunology, University of Toledo College of Medicine, Toledo, Ohio, USA;* [2]*Department of Dermatology, University of Texas Southwestern Medical Center, Dallas, Texas, USA and* [3]*Division of Molecular Biomedicine for Pathogenesis, Center for Disease Biology and Integrative Medicine, University of Tokyo, Tokyo, Japan*

Correspondence: Akira Takashima, Department of Medical Microbiology and Immunology, University of Toledo College of Medicine, 3000 Arlington Avenue, Toledo, Ohio 43614-5806, USA.
E-mail: akira.takashima@utoledo.edu

Abbreviations: BM, bone marrow; DC, dendritic cell; DX, dextran; LC, Langerhans cell; LPS, lipopolysaccharides; OX, oxazolone; WT, wild type

Received 18 September 2009; revised 2 December 2009; accepted 27 December 2009; published online 11 February 2010

significantly impaired delayed-type hypersensitivity responses to foreign protein antigens in IL-1β-deficient mice (Shornick *et al.*, 1996; Nakae *et al.*, 2001; Nambu *et al.*, 2006). Interestingly, severely attenuated contact hypersensitivity responses were also observed in caspase-1-deficient mice (Antonopoulos *et al.*, 2001; Watanabe *et al.*, 2007) and in wild-type (WT) mice after administration of neutralizing antibodies against IL-1β, but not against IL-1α (Enk *et al.*, 1993). Although relative contributions between IL-1α and IL-1β remain somewhat controversial, it is reasonable to state that IL-1 being produced in the skin serves as an indispensable proinflammatory mediator. Nevertheless, little information has been available with regard to spatiotemporal regulation of IL-1 production in living animals.

We recently found rapid and profound IL-1β promoter activation in DCs upon *in vitro* exposure to a variety of chemical and biological agents. In those studies, we used a 4.1 kb 5′-flanking fragment isolated from the murine IL-1β gene to drive the expression of the yellow fluorescence protein gene in a stably transduced DC clone. The resulting DC biosensor clone has enabled us to perform unbiased screening of a wide variety of natural and synthetic compounds for their potential to trigger IL-1β production (Mizumoto *et al.*, 2005). In this study, we sought to construct an *in vivo* reporter system by using the same IL-1β promoter to drive the expression of a fluorescence marker gene. The resulting transgenic mice, in combination with advanced intravital optical imaging technologies, have indeed allowed us to directly visualize IL-1β promoter activation in living animals. In this study, we report spatial regulation of IL-1β promoter activation, as well as the cellular identities and motile activities of IL-1β-producing cells in inflamed skin in an animal model.

RESULTS AND DISCUSSION

Detection of IL-1β promoter activation in hapten-painted skin

We generated a transgenic mouse line expressing the red fluorescent protein DsRed gene under the control of the 4.1 kb mouse IL-1β promoter. The pIL1-DsRed transgenic mice showed no apparent developmental abnormality. Topical application of a skin sensitizer, oxazolone (OX), a standard protocol widely used to trigger IL-1-dependent activation of epidermal-resident LCs (Cumberbatch *et al.*, 1997), triggered time-dependent IL-1β mRNA expression in the pIL1-DsRed transgenic mice (Figure 1a). The magnitude of IL-1β mRNA induction in these mice was comparable to that observed in WT mice (Figure 1b). Tissue extracts prepared from OX-painted ear skin showed large amounts of IL-1β proteins as measured by ELISA (Figure 1c). Time-course experiments showed rapid (6 hours) and robust IL-1β protein production in OX-painted skin with peak responses observed at 24 hours. Once again, pIL1-DsRed transgenic mice were indistinguishable from WT mice in the magnitude or kinetics of OX-induced IL-1β protein expression. No IL-1β mRNA or protein induction was detected after topical application of vehicle alone.

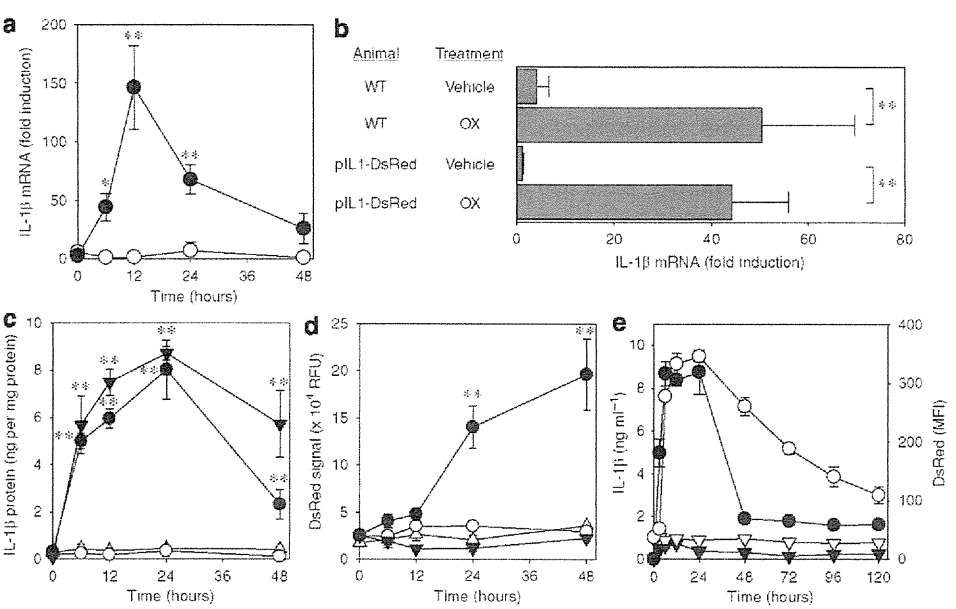

Figure 1. Correlation between DsRed fluorescence signals and IL-1β production. (**a**) pIL1-DsRed transgenic mice were treated by topical application of OX (closed symbols) or vehicle alone (open symbols). At the indicated time points, the ear skin samples were examined for IL-1β mRNA expression by real-time PCR. (**b**) Ear skin samples were isolated from WT mice or pIL1-DsRed transgenic mice 6 hours after topical application of OX or vehicle alone. The samples were then examined for IL-1β mRNA expression by real-time PCR. (**c**) WT mice (triangles) or pIL1-DsRed transgenic mice (circles) received topical application of OX (closed symbols) or vehicle alone (open symbols). At the indicated time points, the ear skin samples were examined for IL-1β protein levels by ELISA. (**d**) The same ear extract samples analyzed in panel **b** were tested for DsRed fluorescence signals by spectrophotometric analyses. (**e**) BM-DCs propagated from pIL1-DsRed transgenic mice were pulsed with LPS (circles) or vehicle alone (triangles) for 1 hour. After extensive washing, the cells were cultured for the indicated periods in the absence of LPS to measure IL-1β release into the culture supernatants by ELISA (closed symbols) and DsRed expression (mean fluorescence intensity, open symbols) by flow cytometry. Data shown are the means ± SD from three mice per group (**$P < 0.01$).

To determine whether OX treatment also triggered IL-1β promoter-driven DsRed expression, we measured DsRed fluorescence signals in the same ear skin extracts by a spectrophotometer (Figure 1d). Minimal fluorescence signals were detected in ear skin samples treated with vehicle alone. OX treatment markedly increased DsRed signals in 12–24 hours, with peak responses observed at 48 hours. No significant increase in DsRed signals was detected in WT mice even after OX application, indicating specificity. Although the time kinetics for DsRed induction in skin showed a lag time of 6–12 hours behind IL-1β protein expression, which presumably represents the interval required for polymerization of newly synthesized DsRed proteins, our findings validated the subsequent use of the newly generated transgenic mice for studying IL-1β promoter activation in living animals.

The discordance of time kinetics observed between IL-1β protein production and DsRed expression might prevent us from studying the resolution phase of inflammatory responses. To test this, we compared time kinetics of IL-1β protein production versus DsRed signals in bone marrow–derived DCs (BM-DCs) propagated from pIL1-DsRed transgenic mice (Figure 1e). Short-term pulsing with LPS induced rapid IL-1β protein production within 3 hours; IL-1β levels reached a peak at 6–24 hours and then declined sharply at 48 hours, with a relatively short half-life of 24 hours. By contrast, DsRed signals became detectable only at 6 hours, reached a plateau at 12–24 hours, and then declined more slowly, with an estimated half-life of 24–48 hours. These observations imply a major limitation of our experimental system; i.e., one can assess IL-1β protein production by measuring DsRed fluorescence signals only in the induction phase of inflammation.

Surface phenotypes of DsRed$^+$ cells emerging in inflammatory skin lesions

Enk and Katz (1992) reported almost two decades ago that topical application of contact sensitizers triggered rapid and abundant IL-1β mRNA expression in the epidermal compartment and that IL-1β mRNA was expressed predominantly by an MHC class II–positive epidermal cell fraction, i.e., LCs. The latter observation was made by measuring IL-1β mRNA expression by semiquantitative RT-PCR in epidermal cell suspensions after complement-mediated deletion of MHC class II–positive cells. To directly examine cell-surface phenotypes of cells expressing DsRed fluorescence signals, we harvested ear skin samples at different time points after OX painting, separated the epidermis from underlying dermis by enzymatic treatment, and then prepared single-cell suspensions from the two compartments independently. Flow cytometric analyses of the resulting epidermal cell suspensions revealed a time-dependent increase in the number of DsRed$^+$ cells, with a sharp peak observed at 48 hours after OX treatment (Figure 2a). Most (>85%) of the DsRed$^+$ cells isolated from the epidermis were found to express a common leukocyte marker, CD45, although a small fraction of CD45$^-$ epidermal cells (i.e., keratinocytes) showed DsRed signals at modest levels (Figure 2b). The CD45$^+$ cells recovered before OX treatment, which represent two epidermal resident leukocyte populations (LCs and epidermal γδ T cells), expressed no detectable DsRed signals constitutively. The number of CD45$^+$ cells markedly increased after OX treatment, perhaps reflecting immigration of inflammatory leukocytes into the epidermal compartment. Importantly, DsRed signals were clearly detected in large fractions (53–61%) of the CD45$^+$ cells recovered after OX painting. Virtually all DsRed$^+$/CD45$^+$ cells expressed CD11b, which is displayed by many leukocyte subsets of the myeloid lineage (Figure 2c). More than 75% of the DsRed$^+$/CD45$^+$ cells also displayed high levels of Gr-1, a conventional marker of neutrophils. Although the overall phenotype of the CD45$^+$/CD11b$^+$/Gr-1^{high} cells instantaneously suggested their identity as granulocytes, some of them may represent "myeloid suppressors" (which inhibit DC-induced T-cell activation) (Gabrilovich and Nagaraj, 2009) and/or "inflammatory monocytes" (which give rise to DCs) (Auffray *et al.*, 2009). The remaining DsRed$^+$/CD45$^+$/Gr-1^{low} cells probably included monocytes/macrophages and certain DC subsets. In fact, F4/80 and MHC class II molecules were detected on relatively small fractions of the CD45$^+$/DsRed$^+$ cells (Figure 2c). These results implied that DsRed signals were produced by selected subsets of myeloid inflammatory leukocytes infiltrating the epidermis after OX painting.

Dermal cell suspensions prepared in parallel also showed time-dependent increases in the number of DsRed$^+$ cells with a sharp peak at 48 hours (Figure 3a). Virtually all of the DsRed$^+$ cells recovered from the dermal compartment also expressed CD45 (Figure 3b). Moreover, the CD45$^+$/DsRed$^+$ cells uniformly displayed CD11b, indicating their myeloid origin (Figure 3c). Interestingly, only small fractions (18–20%) of the DsRed$^+$/CD45$^+$ cells expressed Gr-1 at high levels, in contrast to our observations of the epidermal cell suspensions. Instead, Gr-1 was detected at low levels in a majority (65–75%) of the DsRed$^+$/CD45$^+$ cells. Similarly, F4/80 and MHC class II were detected in 36–46% and 10–12% of the DsRed$^+$/CD45$^+$ cells, respectively. Thus, it seems that DsRed signals were expressed by relatively heterogeneous leukocyte subsets of myeloid origin (i.e., granulocytes, monocytes/macrophages, and DCs) in the dermal compartment after OX painting.

Detection of DsRed$^+$ cells in fixed skin samples

In the next set of experiments, we sought to directly visualize the cells expressing DsRed fluorescence signals in the tissue. For this purpose, we harvested ear skin at different time points after OX application, fixed the samples with paraformaldehyde, and then examined the whole-ear specimens under a macro-zoom fluorescence microscope. Consistent with our findings from spectrophotometric and flow cytometric analyses, very few DsRed$^+$ cells were found in skin samples harvested before OX painting from pIL1-DsRed transgenic mice. DsRed$^+$ cells became clearly detectable 12 hours after OX treatment (Figure 4a). Interestingly, most DsRed$^+$ cells emerged as clusters around hair follicles. The number of DsRed$^+$ cells increased thereafter, reaching a peak at 48 hours. Consistent with our observations in spectrophotometry and flow cytometry analyses, the DsRed signals

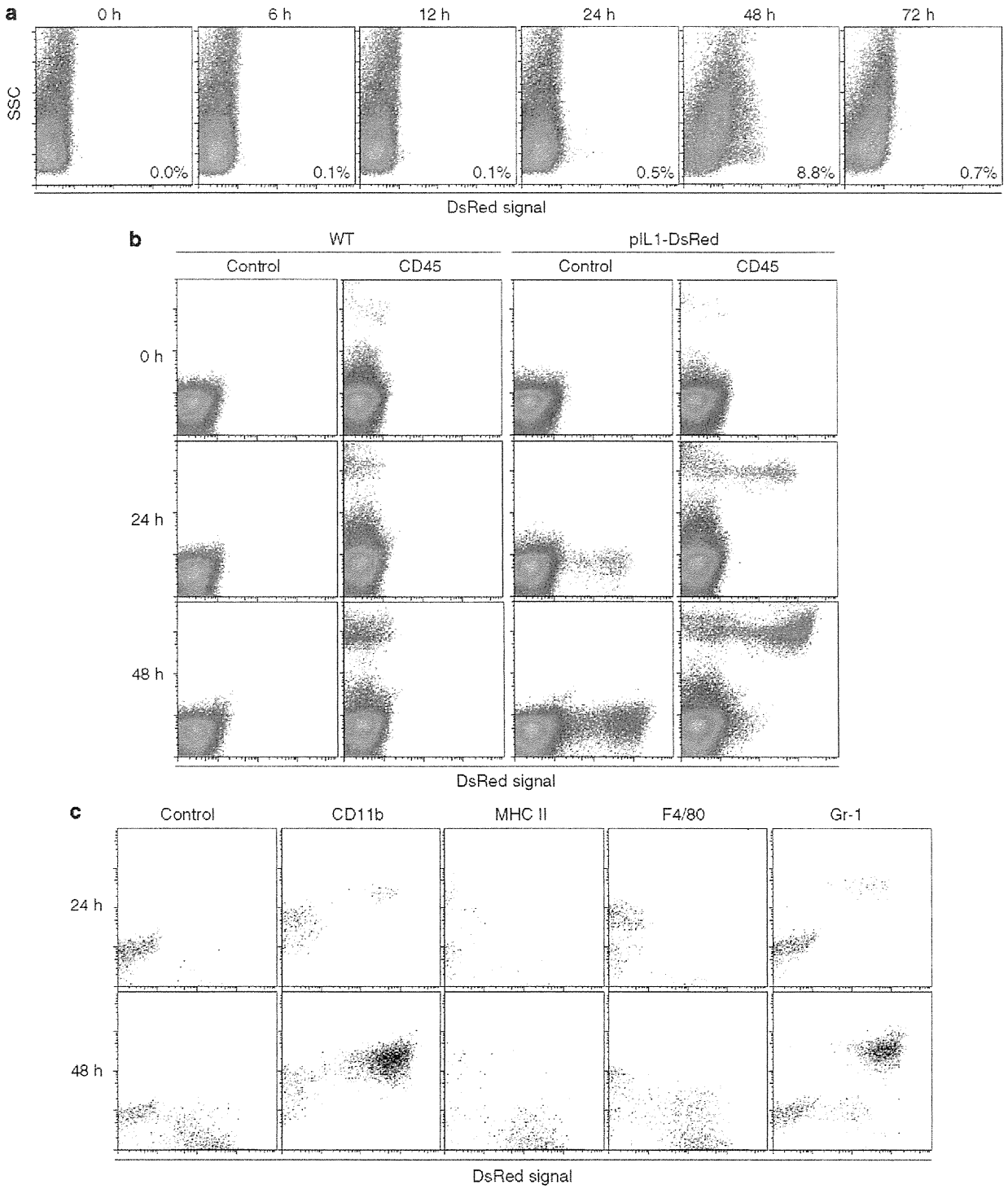

Figure 2. Surface phenotype of DsRed$^+$ cells emerging in the epidermal compartment. (**a**) Epidermal cell suspensions were prepared from the ear skin of pIL1-DsRed transgenic mice at the indicated time points after topical application of OX and examined for DsRed expression. (**b**) Epidermal cell suspensions from WT mice or pIL1-DsRed transgenic mice were also stained with anti-CD45 mAb or isotype-matched control IgG and then examined for expression of CD45 (*y* axis) and DsRed (*x* axis). (**c**) The CD45$^-$ populations in the above experiments were examined for the expression of the indicated surface markers (*y* axis) and DsRed (*x* axis).

declined sharply at 72 hours. No DsRed$^+$ cells were observed in WT mice even after OX painting, again indicating specificity (Figure 4b). Clusters of DsRed$^-$ cells were also observed after topical application of a second contact sensitizer, 2,4-dinitrofluorobenzene (Figure 4c). Moreover, inflammatory skin lesions induced by application

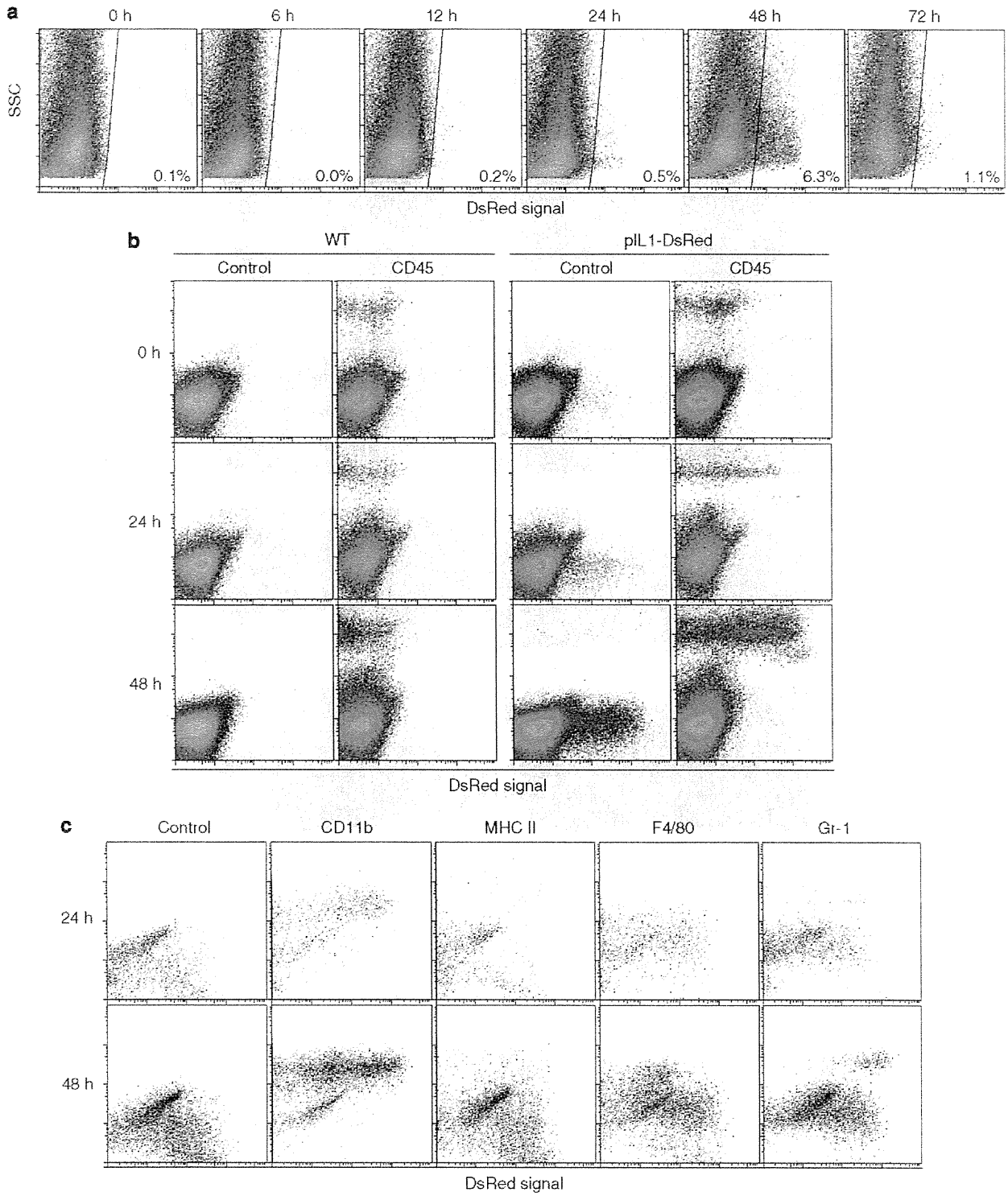

Figure 3. Surface phenotype of DsRed$^+$ cells emerging in the dermal compartment. (**a**) Dermal cell suspensions were prepared from the ear skin of plL1-DsRed transgenic mice at the indicated time points after topical application of OX and examined for DsRed expression. (**b**) Dermal cell suspensions from WT mice or plL1-DsRed transgenic mice were also stained with anti-CD45 mAb or isotype-matched control IgG and then examined for expression of CD45 (*y* axis) and DsRed (*x* axis). (**c**) The CD45$^+$ populations in the above experiments were examined for the expression of the indicated surface markers (*y*-axis) and for DsRed (*x* axis).

of a skin irritant, lactic acid, or by repeated tape stripping were also characterized by the emergence of large numbers of DsRed$^+$ cells.

To record images of DsRed$^+$ cells with higher resolution and to determine their *z*-axis locations, we next examined paraformaldehyde-fixed ear specimens under a confocal

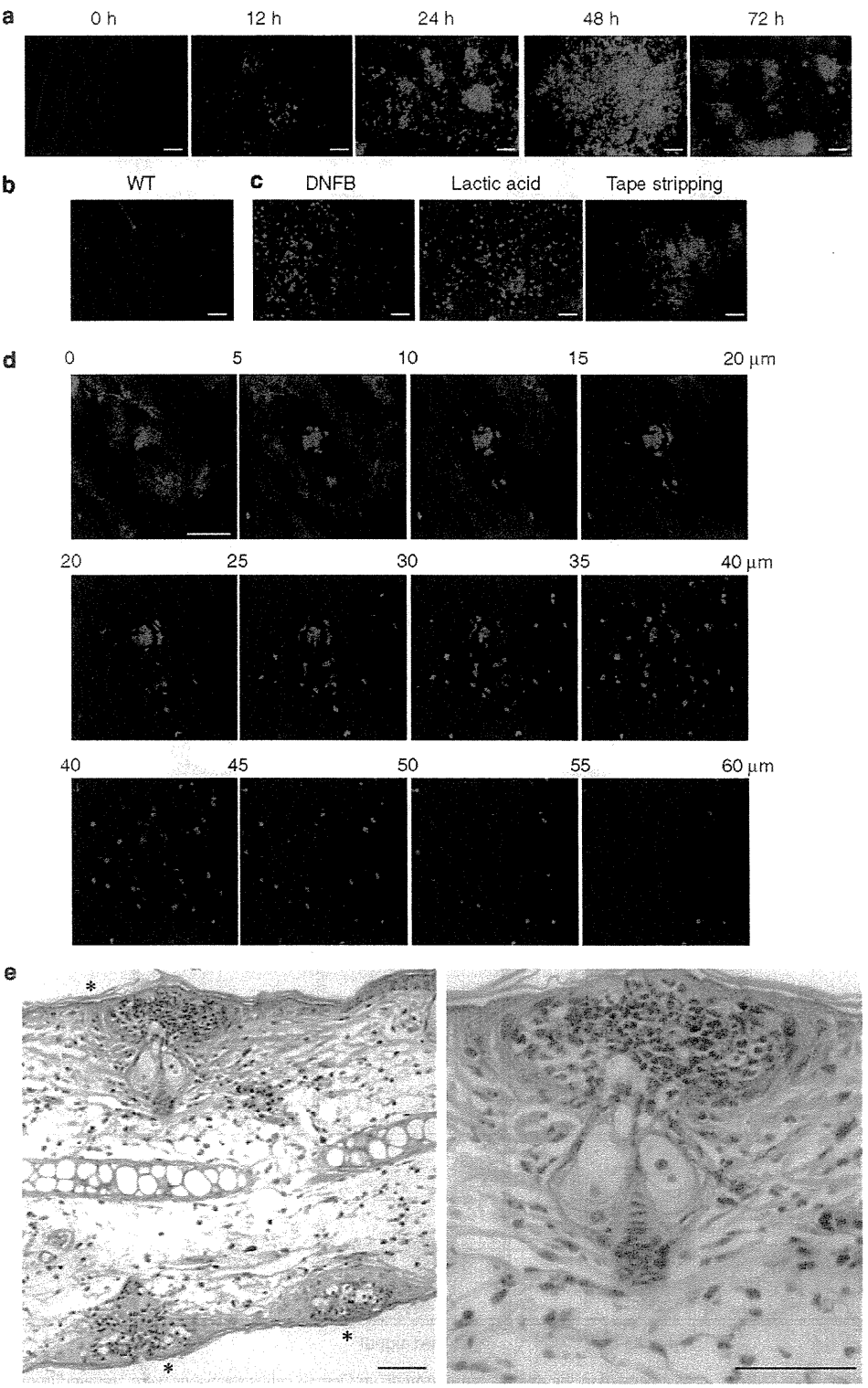

Figure 4. **Emergence and distribution of DsRed$^+$ cells in skin under inflammatory conditions.** (**a**) At the indicated time points after OX treatment of pIL1-DsRed transgenic mice, ear skin samples were harvested. Data shown are images acquired with a macro-zoom fluorescence microscope. (**b**) WT mice were treated with OX, and the ear skin samples harvested at 24 hours were examined under a macro-zoom fluorescence microscope. (**c**) pIL1-DsRed transgenic mice were treated with topical application of 2,4-dinitrofluorobenzene or lactic acid, or with repeated tape stripping. The ear skin samples harvested at 24 hours were examined under a macro-zoom fluorescence microscope. Bar (**a–c**) = 1,000 μm. (**d**) At 24 hours after OX treatment of pIL1-DsRed transgenic mice, the ear skin samples were harvested, fixed with 2% paraformaldehyde, and then examined under a confocal microscope. Data shown are compiled *x–y* plane images of DsRed$^+$ cells in the indicated 5 μm *z*-axis depth range from the skin surface. (**e**) Hematoxylin and eosin histology of ear skin samples harvested 24 hours after OX painting. Asterisks indicate hair follicles. Bar = 100 μm.

microscope (Figure 4d). Sequential *x–y* plane images scanned at different *z*-axis levels revealed that some keratinocytes showed DsRed fluorescence signals at marginal levels, producing cobblestone-like patterns in the epidermal compartment (up to ~20 μm in depth from the skin surface). Within the epidermis, DsRed$^-$ signals appeared as small aggregates associated with hair shafts, which were readily identifiable with autofluorescence signals. Interestingly, a small number of dendritic-shaped epidermal cells characterized by extension of several elongated processes exhibited strong DsRed signals. In the dermal compartment, most DsRed$^+$ cells were preferentially found around hair follicles at the *z*-axis depth range from ~20 to ~50 μm. Hematoxylin and eosin staining of vertical sections revealed multiple foci of dense infiltration by mononuclear and polymorphonuclear leukocytes around hair follicles in OX-treated ear skin (Figure 4e).

Real-time visualization of motile behaviors of DsRed$^-$ cells in living animals

To visualize IL-1β-producing cells in living tissue, we anesthetized pIL1-DsRed transgenic mice and recorded static 3D images of DsRed$^+$ cells in the OX-painted ear skin under a confocal microscope. Once again, compiled *x–y* plane images showed clusters of DsRed$^+$ cells preferentially around hair follicles (Figure 5a), and *z*-axis scanning and 360° rotation of the images further revealed that most of the DsRed$^+$ cells were located in the dermal compartment (see Supplementary Movies S1–S3 online). Once again, relatively small numbers of DsRed$^+$ cells showing a characteristic morphology of LCs were observed in the epidermal compartment (Supplementary Movie S2). Thus, we concluded that inflammatory leukocytes account for a majority of DsRed$^+$ cells emerging in the inflamed skin of living animals.

A key question was whether the observed clusters of DsRed$^+$ cells around hair follicles might be caused simply by particularly "leaky" blood vessels in those anatomical sites. To test this, we intravenously injected FITC-dextran (DX) into pIL1-DsRed transgenic mice 24 hours after OX painting on the ear. As shown in Figure 5b, significantly dilated blood vessels were readily observed in OX-treated skin, whereas leakage of FITC-DX was noticed only occasionally. Another concern was whether the experimental procedures used for confocal imaging (i.e., laser excitation, tissue handling, and

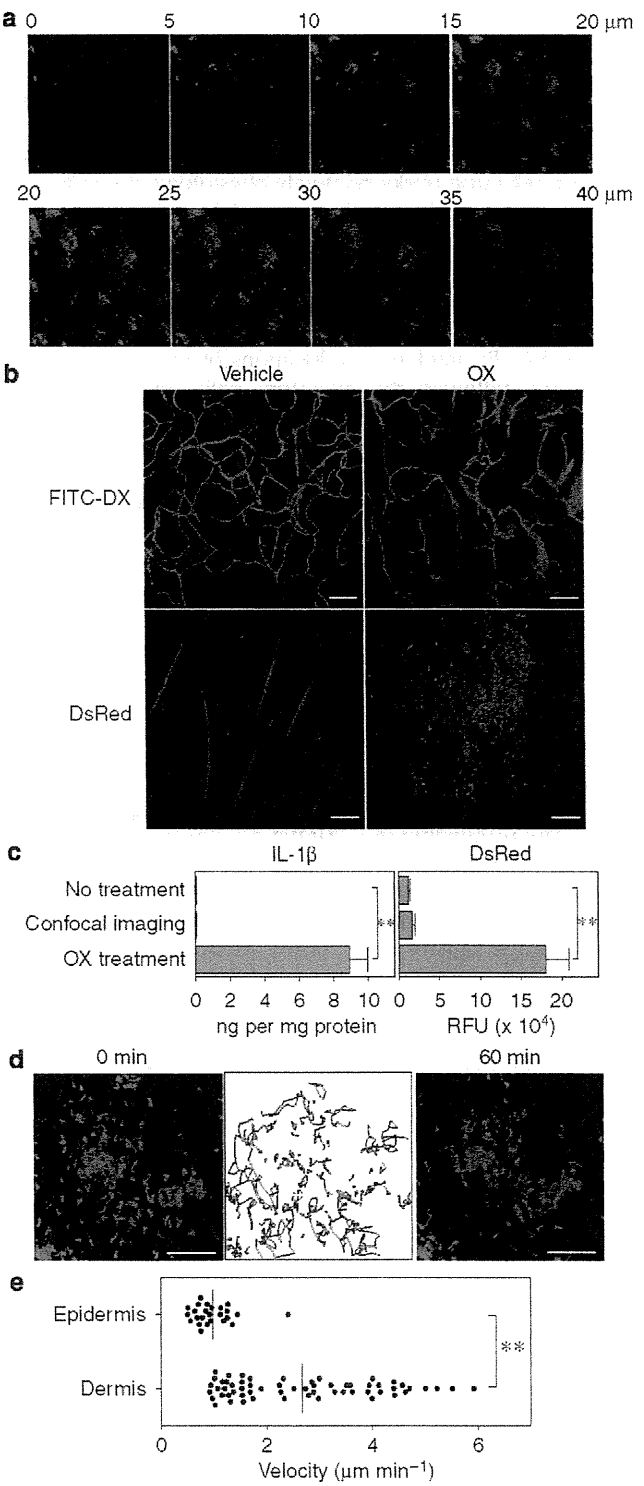

Figure 5. Location and movement of DsRed$^+$ cells emerging in inflammatory skin lesions. (**a**) At 24 hours after OX treatment, pIL1-DsRed transgenic mice were anesthetized and examined under a confocal microscope. Data shown are compiled *x–y* plane images of DsRed$^+$ cells in the indicated 5 μm *z*-axis depth range from the skin surface. Bar = 100 μm. (**b**) At 24 hours after topical application of OX or vehicle alone, FITC-DX was intravenously injected into pIL1-DsRed transgenic mice to visualize blood vessels. The images were recorded 5 minutes after FITC-DX injection. Bar = 100 μm. (**c**) At 24 hours after 30-minute-long confocal imaging sessions or OX treatment, ear skin extracts were examined for IL-1β protein and DsRed signals. Data shown are the means ± SD from three mice per group (**$P<0.01$). (**d**) At 24 hours after OX treatment, pIL1-DsRed transgenic mice were anesthetized to record confocal fluorescence images every 2 minutes for 60 minutes. The images represent the locations of DsRed$^+$ cells at the indicated time points (left and right panels) with migratory paths of individual DsRed$^+$ cells (middle panel). Bar = 100 μm. (**e**) The velocity of each DsRed$^+$ cell was calculated from the above tracking experiments. Velocity values were then compared between the epidermal compartment (up to 18 μm from the skin surface) and the dermal compartment (18–35 μm from the skin surface). Bars indicate mean velocity values (**$P<0.01$).

administration of anesthetics) would deliver pathogenic signals to the imaging site, thereby causing artificial inflammatory responses. To test this possibility, we recorded 3D images in the ear of a pIL1-DsRed transgenic mouse and determined whether such procedures would cause immediate or delayed skin inflammation. In the absence of OX application or other proinflammatory stimuli, very few motile DsRed$^+$ cells were observed at the end of continuous time-lapse imaging up to 60 minutes (data not shown). Moreover, we failed to detect significant IL-1β protein production or DsRed expression even 24 hours after 30-minute imaging sessions (Figure 5c). These observations imply that our confocal imaging protocol enables intravital visualization of IL-1β production under relatively physiological conditions.

To assess motile activities of IL-1β-producing cells, we next recorded 3D images of DsRed$^+$ cells every 2 minutes for 60 minutes. Time-lapse videos generated from these data sets showed that DsRed$^+$ cells constantly displaced the cell bodies via amoeba-like motile behavior (Supplementary Movie S4). By tracking *x*–*y* locations of individual DsRed$^+$ cells, we followed the migratory paths of DsRed$^+$ cells within the 60-minute period (Figure 5d). Interestingly, DsRed$^+$ cells seemed to be more motile in the dermis than in the epidermis (Supplementary Movies S5 and S6). In fact, the mean velocity among DsRed$^+$ cells was significantly higher in the dermal compartment ($2.7 \pm 1.4\,\mu m\,min^{-1}$, $n = 60$) than in the epidermal compartment ($1.0 \pm 0.4\,\mu m\,min^{-1}$, $n = 25$) (Figure 5e). Our intravital time-lapse imaging experiments have demonstrated that myeloid leukocytes, which presumably produce IL-1β, crawl through the extracellular matrix around hair follicles in inflamed skin.

Concluding remarks

In this study, we developed a simple experimental system to directly visualize IL-1β promoter activation in living animals. Abundant production of IL-1β mRNA and protein, as well as robust DsRed expression, became detectable in the skin after topical application of contact sensitizers. Flow cytometric and confocal imaging experiments revealed that DsRed fluorescence signals were mostly associated with CD45$^+$/CD11b$^+$ myeloid leukocytes crawling around hair follicles. Our findings may first seem to be contradictory to the previous report that an MHC class II–positive epidermal cell fraction (i.e., LCs) accounted for a majority of IL-1β mRNA detected by RT-PCR after application of contact sensitizers (Enk and Katz, 1992). It should be stated here that they examined IL-1β mRNA expression only in the epidermal compartment. Moreover, we also observed that some DsRed$^+$ epidermal cells exhibited the characteristic phenotype and morphology of LCs. Thus, it seems reasonable to conclude that LCs represent one, but not the only, IL-1β-producing epidermal cell population in inflamed skin.

Somewhat unexpected was our finding of profound entry of DsRed$^-$/CD11b$^-$/Gr-1^{high} leukocytes into both epidermal and dermal compartments. In this regard, Peters *et al.* (2008), using transgenic mice expressing the enhanced green fluorescence protein gene under the control of the lysozyme M promoter, recently demonstrated a rapid and sustained accumulation of CD11b$^+$/Gr-1^{high} neutrophils (expressing no detectable MHC class II or F4/80) at the bite sites of *Leishmania*-infected sand flies. We now show that DsRed$^+$/CD11b$^-$/Gr-1^{high} leukocytes emerge and crawl around hair follicles in inflamed skin. It remains to be determined whether those leukocytes are derived from progenitors residing in hair follicles, which serve as a reservoir for various stem cell populations (Moore and Lemischka, 2006; Fuchs, 2007), or whether they simply exit the circulation preferentially through hair follicle–associated blood vessels. Nevertheless, this study now provides an important piece of information with regard to leukocyte trafficking to and within inflamed skin.

It is equally important to point out the major weaknesses of our study. First, cells expressing DsRed fluorescence signals do not necessarily represent cells producing biologically active 18 kDa IL-1β protein, because 31 kDa pro-IL-1β protein requires caspase-1-dependent cleavage. In this regard, our approach resembles the recent use of human IL-1β promoter for driving luciferase gene expression (Li *et al.*, 2008). The resulting transgenic mice were then monitored for luciferase expression by intravital bioluminescent imaging in a zymosan-induced arthritis model, an LPS-induced acute peritonitis model, and an OX-induced contact dermatitis model. Although their experimental system enabled real-time monitoring of luciferase activities in affected organs, its spatial resolution was far below the level that we achieved with confocal microscopy. Second, IL-1β mRNA and protein expression was readily detected within 6 hours after OX application, whereas DsRed fluorescent signals became detectable 12–24 hours after the same treatment. This apparent time lag probably represents the time interval required for tetramerization of newly synthesized DsRed molecules. One should be able to overcome this technical limitation by using different fluorescence proteins that emit fluorescence signals in monomeric forms. Likewise, DsRed signals remained at measurable levels even after IL-1β protein became almost undetectable—this discordance in time kinetics, which probably reflects the 24–48 hour difference observed in the half-life between IL-1β and DsRed, represents a limitation of our assay system, especially for studying IL-1β-producing cells in the resolution phase of skin inflammation.

In conclusion, the experimental system developed in this study has allowed us to directly monitor the number, phenotype, location, and movement of IL-1β-producing cells in inflamed skin in living animals with relatively high spatial resolution. Recent advances in confocal microscopy, multiphoton laser scanning microscopy, and green fluorescence protein transgenic and knock-in animals have made it possible to visualize the motile behavior of different leukocyte subsets in lymphoid and epithelial tissues (Germain *et al.*, 2006). Our approach now adds another dimension to such intravital imaging studies by providing key information on cellular function.

MATERIALS AND METHODS

Construction of pIL1-DsRed transgenic mice

A 1.2 kb rabbit β-globin gene containing a noncoding intron/exon was obtained by digesting the pSG-1 expression vector with *Bam*HI

and *Xho*I (Toyonaga *et al.*, 1994; Miyazaki *et al.*, 2001). The fragment was subcloned into the *Bam*HI/*Xho*I site of pBK-CMV (Stratagene, La Jolla, CA) to produce the plasmid pBK-CMV-SG. To generate a red fluorescent protein-expressing vector, a PCR fragment was amplified from pDsRed-Express-DR plasmid (Clontech, Palo Alto, CA) using the primer set 5′-GGGAATTCCGG TCGCCACCATGGCCTC-3′ and 5′-GGAGATCTACACATTGATCC TAGCAGAAG-3′ and was subsequently ligated into a TA-cloning vector, pCR4-TOPO (Invitrogen, Carlsbad, CA), and then subcloned between the *Eco*RI and the *Bgl*II sites of pBK-CMV-SG. The resulting vector, pBK-CMV-SG-Red, carried a CMV immediate early promoter upstream of the β-globin intron/exon-RFP fusion gene. The CMV promoter region was removed by digestion with *Vsp*I and *Nhe*I, followed by blunting of both ends with Klenow fragment and self-ligation. The 4,138-bp *Bam*HI fragment of the murine IL-1β promoter was inserted into the *Bam*HI site to generate the plasmid pBK-SG-IL-1β-Red (Godambe *et al.*, 1995). Plasmid pBK-SG-IL-1β-Red was digested with *Sal*I and *Not*I to clear the vector sequences, and the transgene fragment was purified by Elutip-D (Schleicher and Schuell, Keene, NH). The resulting DNA was microinjected into fertilized eggs of C57BL/6 mice. Transgene expression was determined by genomic PCR for DNA isolated from tail biopsies with specific primers, 5′-TGCTGG TTGTTGTGCTGTCTCATC-3′ and 5′-CACGTACACCTTGGAGCCG TACTG-3′. The screening results were subsequently confirmed at the protein level by testing the expression of DsRed fluorescence signals by peripheral blood mononuclear cells after *in vitro* stimulation with LPS. Transgene-positive mice were bred with WT C57BL/6 mice, and heterozygous offspring were used in this study.

Measurement of IL-1β mRNA and protein expression in skin samples

To measure IL-1β mRNA expression, total RNA was isolated from freshly procured ear skin samples using TRIzol reagent (Invitrogen) and the RNeasy Plus Mini Kit (Qiagen, Valencia, CA). Corresponding cDNA was prepared using the SuperScript III First-Strand System Kit (Invitrogen), and real-time PCR was performed using a LightCycler instrument (Roche Applied Science, Indianapolis, IN) with QuantiTect SYBR Green PCR Master Mix (Qiagen) and specific primers for IL-1β (SA Biosciences, Frederick, MD). The amount of IL-1β mRNA was determined relative to glyceraldehyde-3-phosphate dehydrogenase mRNA using the comparative cycle threshold numbers method. Tissue extracts were prepared from ear skin samples using the T-PER Tissue Protein Extraction Reagent supplemented with Halt Protease Inhibitor Cocktail (Thermo Scientific, Rockford, IN). Protein concentration was determined using the BCA assay kit (Thermo Scientific). IL-1β protein levels were examined using an ELISA kit (R&D Systems, Minneapolis, MN), and DsRed fluorescence intensities were measured using the FLUOstar Omega microplate reader (BMG Labtech, Chicago, IL).

Skin inflammation models

Mice received topical application of 1.25% OX (Sigma-Aldrich, St Louis, MO), 0.5% 2,4-dinitrofluorobenzene (MP Biomedicals, Solon, OH), or 90% lactic acid (Sigma-Aldrich) on their right ears using our standard protocol (Nishibu *et al.*, 2006). The treated ears showed statistically significant ($P<0.01$) swelling compared with the left ears of the same animals painted with vehicle alone. Skin inflammation was also induced mechanically by repeated (10 times) tape stripping (Holzmann *et al.*, 2004).

Measurement of IL-1β release and DsRed expression in BM-DCs

BM-DC cultures were generated from pIL1-DsRed transgenic mice in complete RPMI 1640 supplemented with 10 ng ml^{-1} murine granulocyte-macrophage colony-stimulating factor (Matsushima *et al.*, 2009). BM-DCs were pulsed for 1 hour with 300 ng ml^{-1} LPS, washed extensively, and then cultured for various periods in the absence of added LPS. The cells and culture supernatants were examined for DsRed expression and IL-1β protein, respectively.

Optical imaging of DsRed fluorescence signals

For conventional imaging experiments, freshly procured ear skin specimens were fixed with 2% paraformaldehyde for 30 minutes at room temperature and then examined for DsRed fluorescence signals under an MVX10 MacroView system (Olympus, Melville, NY) or a TCS SP5 confocal microscope (Leica Microsystems, Bannockburn, IL). For intravital imaging experiments, the mice were anesthetized with intraperitoneal injection of an anesthetic cocktail (ketamine, xylaxine, and acepromazine) and placed on an imaging stage to mount the tip of the ear, with the ventral side down, to record images of DsRed$^+$ cells under a TCS SP5 confocal microscope controlled by LAS AF Lite software (Leica Microsystems) as described previously (Nishibu *et al.*, 2006). We typically scanned tissues with *x*, *y*, *z* volumes ($387.5 \times 387.5 \times 60$ or $775 \times 775 \times 80$ μm) at 1 μm *z*-steps to create 3D image sets. *Stratum corneum*–associated autofluorescence signals were used as a marker to define the epidermal compartment, i.e., 20 μm from the outermost surface of the *stratum corneum*. Blood vessels were visualized by intravenous injection of 20 mg ml^{-1} of FITC-DX (70 kDa, Sigma-Aldrich). In time-lapse imaging experiments, 3D images were recorded every 2 minutes for 60 minutes and then analyzed using ImageJ (National Institutes of Health) and Photoshop software (Adobe, San Jose, CA). Tracking of DsRed$^-$ cells in living animals was performed with MetaMorph software (Molecular Devices, Sunnyvale, CA). Construction of the pIL1-DeRed transgenic mouse line and its use in imaging experiments were approved by the institutional review boards at the University of Texas Southwestern Medical Center and the University of Toledo College of Medicine, respectively, and all animal experiments were conducted according to guidelines of the National Institutes of Health.

Flow cytometric analyses

Epidermis was separated from ear skin with 0.5% dispase II (Roche Diagnostics, Indianapolis, IN) for 45 minutes at 37 °C. The epidermis was further treated with 0.3% trypsin (Worthington, Lakewood, NJ) in the presence of 0.1% DNase I (Roche Diagnostics) for 10 minutes at 37 °C to prepare single cell suspension. The dermis was minced and incubated for 1 h at 37 °C with 1,000 U ml^{-1} collagenase XI (Worthington), 1,000 U ml^{-1} hyaluronidase IV (Sigma-Aldrich), and 0.1% DNase I. The obtained single-cell suspensions were pretreated for 15 minutes on ice with 5 μg ml^{-1} anti-CD16/CD32 (2.4G2) mAb, and subsequently stained with fluorescence-conjugated mAb for 30 minutes on ice. In addition to isotype-matched controls, the following mAbs were

used: CD11b (M1/70), CD45 (30-F11), IA-IE (2G9), and Gr-1 (RB6-8C5, all purchased from BD Biosciences, Palo Alto, CA), and F4/80 (BM8; eBioscience, San Diego, CA). After the addition of propidium iodide, samples were analyzed with FACSCalibur (BD Biosciences).

Statistical analyses

Differences in measured variables between the experimental and the control groups were assessed with two-tailed Student's *t*-test. Data from time-course experiments were analyzed by analysis of variance and Dunnett's test. All experiments were repeated more than twice to assess reproducibility.

CONFLICT OF INTEREST

The authors state no conflict of interest.

ACKNOWLEDGMENTS

We thank R. Mohr, C. Krout, and R. Lu for technical assistance of imaging experiments; B. Chojnacki, A. Rupp, and J. Baranski for screening and maintenance of animal colonies; and D. Ammons for secretarial assistance. This work was supported by NIH grants (RO1-AI46755, RO1-AR35068, RO1-AR43777, and RO1-AI43232 to AT).

SUPPLEMENTARY MATERIAL

Supplementary material is linked to the online version of the paper at http://www.nature.com/jid

REFERENCES

Antonopoulos C, Cumberbatch M, Dearman RJ *et al.* (2001) Functional caspase-1 is required for Langerhans cell migration and optimal contact sensitization in mice. *J Immunol* 166:3672–7

Auffray C, Sieweke MH, Geissmann F (2009) Blood monocytes: development, heterogeneity, and relationship with dendritic cells. *Annu Rev Immunol* 27:669–92

Cerretti DP, Kozlosky CJ, Mosley B *et al.* (1992) Molecular cloning of the interleukin-1 beta converting enzyme. *Science* 256:97–100

Coeshott C, Ohnemus C, Pilyavskaya A *et al.* (1999) Converting enzyme-independent release of tumor necrosis factor alpha and IL-1beta from a stimulated human monocytic cell line in the presence of activated neutrophils or purified proteinase 3. *Proc Natl Acad Sci USA* 96:6261–6

Cumberbatch M, Dearman RJ, Kimber I (1997) Langerhans cells require signals from both tumour necrosis factor-alpha and interleukin-1 beta for migration. *Immunology* 92:388–95

Dinarello CA (2009) Immunological and inflammatory functions of the interleukin-1 family. *Annu Rev Immunol* 27:519–50

Enk AH, Angeloni VL, Udey MC *et al.* (1993) An essential role for Langerhans cell-derived IL-1 beta in the initiation of primary immune responses in skin. *J Immunol* 150:3698–704

Enk AH, Katz SI (1992) Early molecular events in the induction phase of contact sensitivity. *Proc Natl Acad Sci USA* 89:1398–402

Fantuzzi G, Ku G, Harding MW *et al.* (1997) Response to local inflammation of IL-1 beta-converting enzyme-deficient mice. *J Immunol* 158:1818–24

Fuchs E (2007) Scratching the surface of skin development. *Nature* 445:834–42

Gabrilovich DI, Nagaraj S (2009) Myeloid-derived suppressor cells as regulators of the immune system. *Nat Rev Immunol* 9:162–74

Germain RN, Miller MJ, Dustin ML *et al.* (2006) Dynamic imaging of the immune system: progress, pitfalls and promise. *Nat Rev Immunol* 6:497–507

Godambe SA, Chaplin DD, Takova T *et al.* (1995) A novel cis-acting element required for lipopolysaccharide-induced transcription of the murine interleukin-1 beta gene. *Mol Cell Biol* 15:112–9

Holzmann S, Tripp CH, Schmuth M *et al.* (2004) A model system using tape stripping for characterization of Langerhans cell-precursors *in vivo*. *J Invest Dermatol* 122:1165–74

Kupper TS (1990) Immune and inflammatory processes in cutaneous tissues. Mechanisms and speculations. *J Clin Invest* 86:1783–9

Kupper TS, Ballard DW, Chua AO *et al.* (1986) Human keratinocytes contain mRNA indistinguishable from monocyte interleukin 1 alpha and beta mRNA. Keratinocyte epidermal cell-derived thymocyte-activating factor is identical to interleukin 1. *J Exp Med* 164:2095–100

Li L, Fei Z, Ren J *et al.* (2008) Functional imaging of interleukin 1 beta expression in inflammatory process using bioluminescence imaging in transgenic mice. *BMC Immunol* 9:49

Luger TA, Stadler BM, Luger BM *et al.* (1982) Murine epidermal cell-derived thymocyte-activating factor resembles murine interleukin 1. *J Immunol* 128:2147–52

Martinon F, Mayor A, Tschopp J (2009) The inflammasomes: guardians of the body. *Annu Rev Immunol* 27:229–65

Matsushima H, Tanaka H, Mizumoto N *et al.* (2009) Identification of crassin acetate as a new immunosuppressant triggering heme oxygenase-1 expression in dendritic cells. *Blood* 114:64–73

Miyazaki T, Ohura T, Kobayashi M *et al.* (2001) Fatal propionic acidemia in mice lacking propionyl-CoA carboxylase and its rescue by postnatal, liver-specific supplementation via a transgene. *J Biol Chem* 276:35995–9

Mizumoto N, Gao J, Matsushima H *et al.* (2005) Discovery of novel immunostimulants by dendritic-cell-based functional screening. *Blood* 106:3082–9

Moore KA, Lemischka IR (2006) Stem cells and their niches. *Science* 311:1880–5

Nakae S, Naruse-Nakajima C, Sudo K *et al.* (2001) IL-1 alpha, but not IL-1 beta, is required for contact-allergen-specific T cell activation during the sensitization phase in contact hypersensitivity. *Int Immunol* 13:1471–8

Nambu A, Nakae S, Iwakura Y (2006) IL-1beta, but not IL-1alpha, is required for antigen-specific T cell activation and the induction of local inflammation in the delayed-type hypersensitivity responses. *Int Immunol* 18:701–12

Nishibu A, Ward BR, Jester JV *et al.* (2006) Behavioral responses of epidermal Langerhans cells *in situ* to local pathological stimuli. *J Invest Dermatol* 126:787–96

O'Neill LA (2008) The interleukin-1 receptor/Toll-like receptor superfamily: 10 years of progress. *Immunol Rev* 226:10–8

Peters NC, Egen JG, Secundino N *et al.* (2008) *In vivo* imaging reveals an essential role for neutrophils in leishmaniasis transmitted by sand flies. *Science* 321:970–4

Shornick LP, De Togni P, Mariathasan S *et al.* (1996) Mice deficient in IL-1beta manifest impaired contact hypersensitivity to trinitrochlorobenzone. *J Exp Med* 183:1427–36

Sugawara S, Uehara A, Nochi T *et al.* (2001) Neutrophil proteinase 3-mediated induction of bioactive IL-18 secretion by human oral epithelial cells. *J Immunol* 167:6568–75

Takashima A, Bergstresser PR (1996) Impact of UVB radiation on the epidermal cytokine network. *Photochem Photobiol* 63:397–400

Thornberry NA, Bull HG, Calaycay JR *et al.* (1992) A novel heterodimeric cysteine protease is required for interleukin-1 beta processing in monocytes. *Nature* 356:768–74

Toyonaga T, Hino O, Sugai S *et al.* (1994) Chronic active hepatitis in transgenic mice expressing interferon-gamma in the liver. *Proc Natl Acad Sci USA* 91:614–8

Watanabe H, Gaide O, Petrilli V *et al.* (2007) Activation of the IL-1beta-processing inflammasome is involved in contact hypersensitivity. *J Invest Dermatol* 127:1956–63

注目される用語の解説

AIM

新井郷子（東京大学大学院医学系研究科疾患生命工学センター分子病態医科学部門講師）
宮崎　徹（東京大学大学院医学系研究科疾患生命工学センター分子病態医科学部門教授）

AIMはマクロファージが産生する分泌蛋白質

AIMは分化成熟したマクロファージが特異的に産生する3つのSRCR（scavenger receptor cystein-rich）ドメインからなる分泌型蛋白質である。1999年に同定し、マクロファージ自身のアポトーシスを抑制する機能をもつことからapoptosis inhibitor of macrophage（AIM）と命名した（ほかにCD5L、Spα、Api6などの呼称がある）[1]。AIMは分泌型蛋白質であるため、そのアポトーシス抑制機構はおそらく受容体を介したものであると考えられるが、Fasや放射線、ステロイド、または細菌感染、細胞ストレスなど、さまざまなタイプのアポトーシス誘導に対し抵抗性を示すことからも[1,2]、特定のアポトーシス誘導シグナルを阻害するというより、細胞のviabilityを高めているという見方のほうがふさわしいかもしれない。アポトーシス抑制の詳細な分子メカニズムは現在解析中である。

AIMは動脈硬化の病態進行に深く関与する

AIMはマクロファージにおいて核内受容体LXR（liver X receptor）/RXR（retinoid X receptor）ヘテロ二量体の活性化により強く誘導される。LXRは酸化LDLの分解物であるオキシステロールをリガンドとして活性化され、ほかには*ABCA-1*（*ATP-binding cassette, sub-family A, member 1*）や*ApoE*（*apolipoprotein E*）など、細胞外へのコレステロール排出系統にかかわる重要な分子群の遺伝子発現を誘導することが知られている。

高コレステロール血症下では動脈の血管内皮下層における酸化LDL濃度が高まり、掃除屋マクロファージが浸潤して酸化LDLを貪食する。酸化LDLを取り込んだマクロファージは細胞内にコレステロールエステルを溜め込んで泡沫化して膨れ上がり、内皮下層に蓄積していくことで動脈硬化巣形成の礎となるが、そのような細胞は酸化LDLの刺激によりLXRが強く活性化されているために、AIMを非常に強く産生している[3]。そのため、硬化巣マクロファージは、酸化LDLや炎症性サイトカイン類、Fas-Fasリガンド系などの細胞間相互作用、一酸化窒素（NO）などのさまざまなアポトーシス誘導性物質や、局所的な低栄養状態、低酸素状態などの環境悪化に常に曝されているにもかかわらず、アポトーシス抵抗性を示す。このことは硬化巣において泡沫化細胞の蓄積とそれに伴う病巣の炎症反応の持続をもたらし、病態進行の悪化の原因になる。実際に、AIM非存在下では、硬化巣においてマクロファージのアポトーシスの顕著な増加がみられ、さらにそれに

図1　AIMの欠損による動脈硬化の軽減

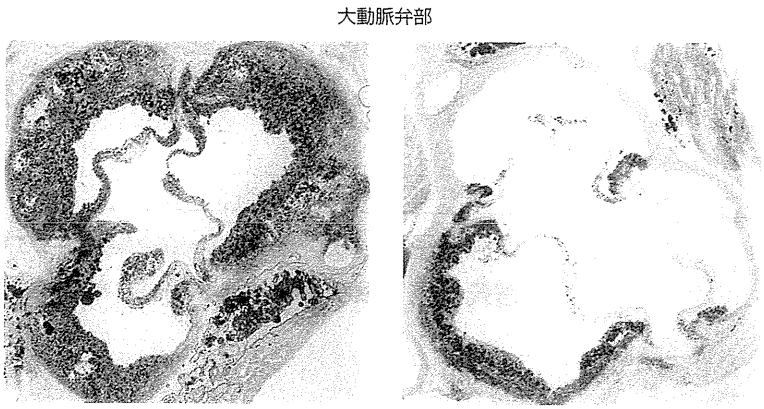

高コレステロール食を12週間与えたマウスに形成された動脈硬化巣

LDLR：LDL受容体　（文献3より引用）

図2　肥満の進行と脂肪細胞によるAIMの取り込み

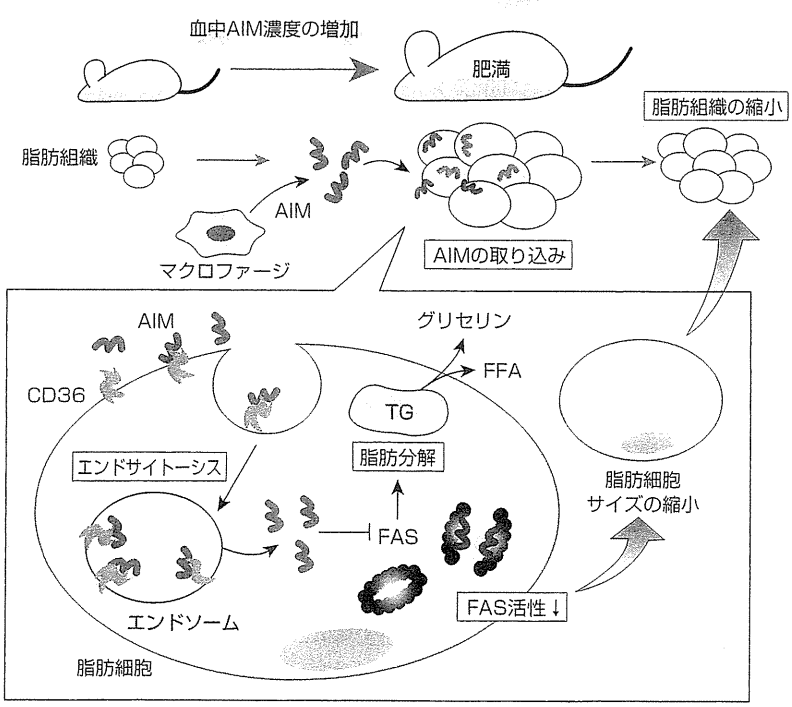

FAS：脂肪酸合成酵素　TG：triglyceride（中性脂肪）　FFA：free fatty acid（遊離脂肪酸）

伴う病巣の炎症反応の軽減により、病態の初期から後期にかけて動脈硬化の著しい軽減が観察されることがAIMを欠損した動脈硬化モデルマウス（*AIM*$^{-/-}$*LDLR*$^{-/-}$マウス）を用いて示されている[3]（**図1**）。

最新トピックス：AIMは脂肪細胞によって取り込まれ、脂肪分解を誘導する

上記の知見に加え、最近われわれは脂肪細胞におけるAIMの新たな機能を発見した[4]（**図2**）。分泌型

蛋白質であるAIMは通常も血中に存在するが、マウスに高脂肪食を与えて肥満化させると血中濃度が急激に上昇する（約5倍程度）。このような肥満誘導下の脂肪組織では、AIMは脂肪細胞によってスカベンジャー受容体であるCD36を介してエンドサイトーシスにより取り込まれる。AIMは細胞内ではエンドソームから放出され、細胞質中の脂肪酸合成酵素（fatty acid synthase；FAS）に結合することでその酵素活性を抑制する。その結果、脂肪細胞において貯蔵していた脂肪の分解が誘導され、グリセロールと遊離脂肪酸（free fatty acid；FFA）として細胞外へ放出される。すなわち、AIMは脂肪分解蛋白質として機能し、脂肪細胞を縮小させる働きをもつ。実際に、AIM非存在下では脂肪分解が抑えられるため、高脂肪食負荷による脂肪細胞の肥大化が促進され、内臓脂肪蓄積量も多くなることがAIM$^{-/-}$マウスを用いて示されている。

今後の展望

AIMはおよそ10年前に同定してから最近まで、その存在意義の問われる謎の多い蛋白質であった。しかしながら近年、メタボリックシンドロームの各疾患におけるAIMの重要性が次々に明らかになりつつある。動脈硬化においては硬化巣の泡沫化マクロファージにアポトーシス抵抗性をもたらせることで病態を悪化させ、肥満脂肪組織においては脂肪分解を誘導することで脂肪細胞を縮小させるいわゆる「痩せ」効果をもつ。そのほかにも、近年注目されている肥満脂肪組織における慢性炎症や、脂肪肝からなる肝機能障害においてAIMがどのような作用を及ぼすのか、解明すべき点が多く残されており、それらは今後のわれわれの課題である。しかしながら、AIMがメタボリックシンドロームの病態生理に深く組み込まれた分子であることは間違いなく、近い将来、AIMの存在を意識したうえでメタボリックシンドロームの全体像を理解することが求められるだろう。

文　献

1)Miyazaki T, Hirokami Y, Matsuhashi N, Takatsuka H, Naito M. Increased susceptibility of thymocytes to apoptosis in mice lacking AIM, a novel murine macrophage-derived soluble factor belonging to the scavenger receptor cysteine-rich domain superfamily. J Exp Med 1999; 189: 413-22.

2)Joseph SB, Castrillo A, Laffitte BA, Mangelsdorf DJ, Tontonoz P. Reciprocal regulation of inflammation and lipid metabolism by liver X receptors. Nat Med 2003; 9: 213-9.

3)Arai S, Shelton JM, Chen M, Bradley MN, Castrillo A, Bookout AL, et al. A role for the apoptosis inhibitory factor AIM/Spα/Api6 in atherosclerosis development. Cell Metab 2005; 1: 201-13.

4)Kurokawa J, Arai S, Nakashima K, Nagano H, Nishijima A, Miyata K, et al. Macrophage-derived AIM is endocytosed into adipocytes and decreases lipid droplets via inhibition of fatty acid synthase activity. Cell Metab 2010; 11: 479-92.

特集 メタボリック症候群と病理

メタボリック症候群におけるAIMの機能

新井郷子*
宮崎 徹*

はじめに

我々はこれまで，マクロファージが特異的に発現する分泌蛋白質であるAIM（apoptosis inhibitor of macrophage）について研究を進めてきた．AIMはマクロファージ自身のアポトーシス抑制機能をもつ蛋白質としておよそ10年前に同定したが，近年，発現誘導機構や新しい機能の解明が進み，AIMがメタボリック症候群に様々な角度から非常に深く関与していることが明らかになった．本稿は，AIMがそのアポトーシス抑制機能により病態に関与する動脈硬化，および最近新たに発見した脂肪細胞におけるlipolysis（脂肪分解）機能について紹介する．本稿をとおしてメタボリック症候群の病態生理について理解を深める一助となることを願う．

Ⅰ．AIMとは

AIMは分化成熟したマクロファージが特異的に産生する3つのSRCR（scavenger receptor cysteine-rich）ドメインからなる分泌型蛋白質である．1999年に同定し，アポトーシスを抑制する機能をもつことからapoptosis inhibitor of macrophage（AIM）と命名した（ほかにCD5L，Spα，Api6などの呼称がある）[1,2]．標的となる細胞としては，現在までに胸腺のダブルポジティブ細胞やNK-T（natural killer-T）細胞，そしてマクロファージ自身がみつかっており[1,3]，特にマクロファージについては多く研究がなされている．AIMは分泌型蛋白質であるため，そのアポトーシス抑制機構はおそらく受容体を介したものであると考えられるが，Fasや放射線，ステロイド，または細菌感染，細胞ストレスなど，様々なタイプのアポトーシス誘導に対し抵抗性を示すことからも[1,4]，特定のアポトーシス誘導シグナルを阻害するというよりも，細胞のviabilityを高めているという見方のほうが相応しいかもしれない．詳細な分子メカニズムは現在解析中である．

最近，上記のほかに新たな標的細胞として脂肪細胞がみつかった[5]．これによりAIMが肥満の進行に伴う脂肪組織の変化に非常に重要な役割を果たしていることが判明したが，この件に関しては，後述Ⅲで紹介する．

発現に関しては，IFNγ（interferon γ）や各種インターロイキン，LPS（lipopolysaccharide），PMA（phorbol-12-myristate-13-acetate）添加などによるマクロファージの刺激では誘導できないことが*in vitro*の実験で示されている[1]．だが近年，核内受容体であるLXR（liver X receptor）/RXR（retinoid X receptor）ヘテロ二量体の活性化により，AIMの発現が強く誘導されることが判明した[2,4,6]．LXRは酸化LDLの分解物であるオキシステロールをリガンドとして活性化され，*ABCA-1*（ATP-binding cassette, sub-family A, member 1）や*ApoE*（apolipoprotein E）など，細胞外へのコレステロール排出系統に関わる重要な分子群の遺伝子発現を誘導することが知られている．動脈硬化巣の泡沫化マクロファージはLXRが強く活性化されているためAIMを高発現しており，このため動脈硬化の病態進行にはAIMが深く関与する[6]．動脈硬化におけるAIMの役割については後述Ⅱで紹介する．

その他，AIMの発現誘導に関する知見として，中性脂肪代謝に重要な酵素であるライソゾーム酸性リパーゼlysosomal acid lipase（LAL）の遺伝子欠損マウスにおいて，肺胞上皮細胞にAIMの発現が非常に強く誘導されるとの報告がある[7]．また，癌遺伝子である*MafB*が*AIM*遺伝子のプロモータを刺激することが肺胞上皮細胞株であるH441細胞を用いた実験で示

*東京大学大学院医学系研究科 疾患生命工学センター分子病態医科学部門

0287-3745/10/¥100/頁/JCOPY

図1　動脈硬化の発生機序
【病変初期段階】：動脈の血管内皮下層に浸潤したマクロファージは酸化LDLを取り込み，泡沫化マクロファージとなり蓄積する．
【増悪期】：病巣の泡沫化マクロファージは蓄積を重ねるとともに，浸潤したT細胞と相互作用し，炎症反応を誘起・確立する．炎症は平滑筋細胞の遊走・増殖を誘導し，線維性プラークの発達を促す．
【後期】：動脈硬化が非常に進行すると，壊死を起こした硬化巣マクロファージから放出された脂溶性物質を含んだ壊死組織であるネクローティック・コアnecrotic core（NC）が形成される．このような組織は脆弱で，血流等で破壊されて内容物が血液中に流出すると血小板の凝集が起こり，血栓が形成される．
（文献8より）

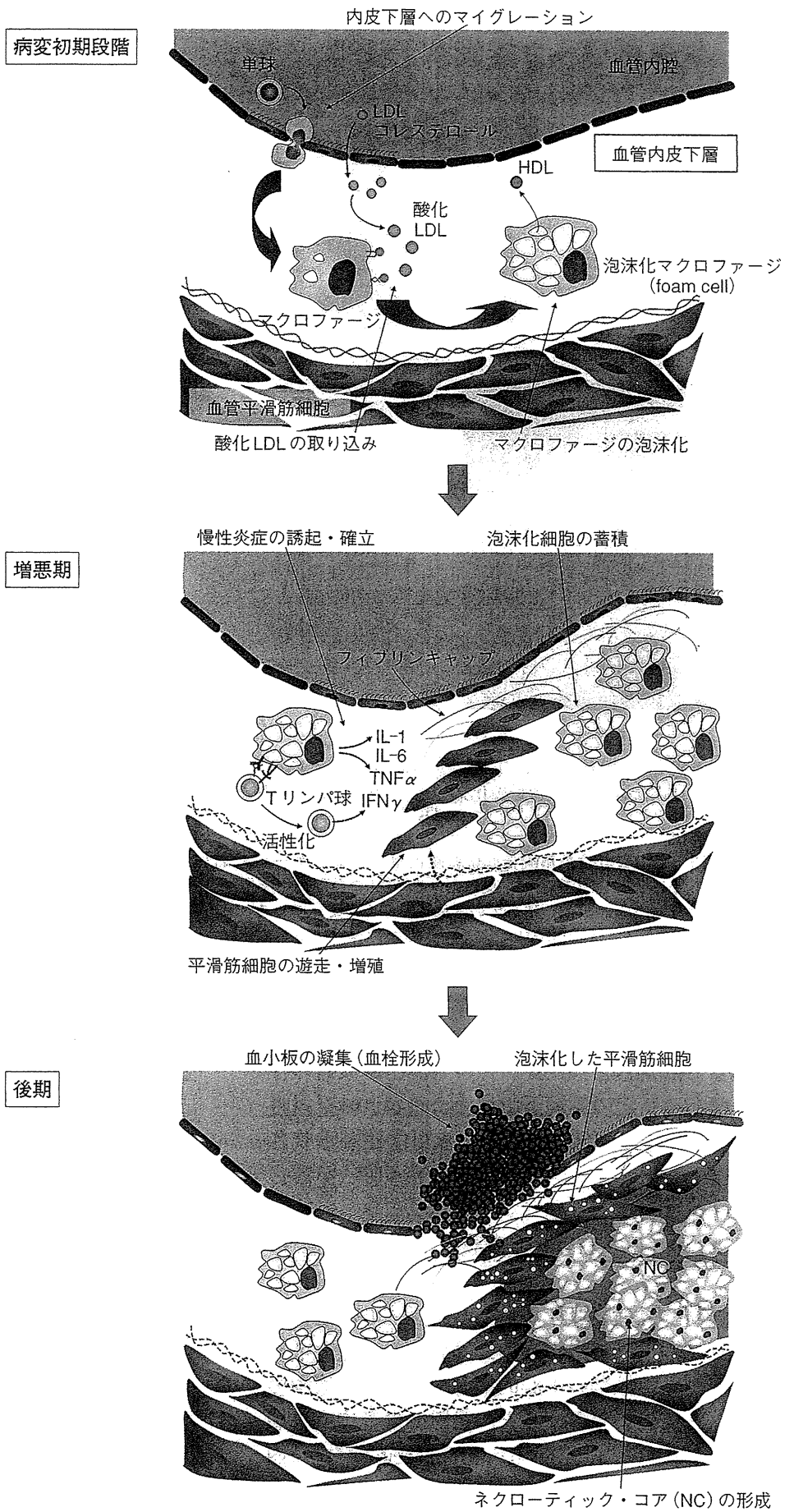

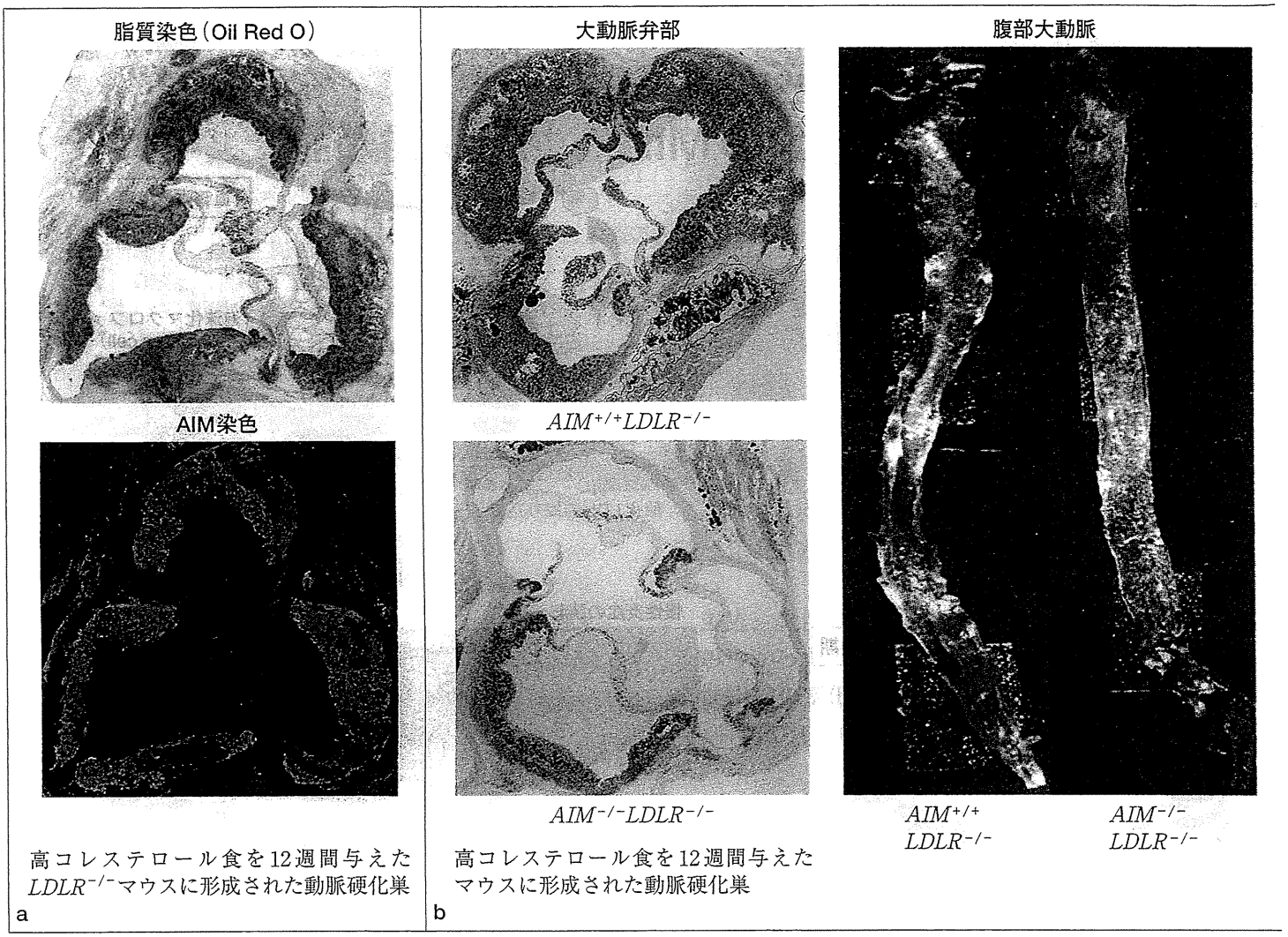

図2　動脈硬化とAIM　a：動脈硬化巣マクロファージにおけるAIMの発現．高コレステロール食を12週間与えた$LDLR^{-/-}$マウスの動脈硬化巣におけるAIMの発現を免疫化学染色にて調べた．Oil Red Oは脂質を赤く染めるので，泡沫化マクロファージが蓄積している部位が赤く染まっている．また同じ箇所が抗AIM抗体（緑色）によって染まっているのがわかる．b：AIMの欠損による動脈硬化の軽減．$LDLR^{-/-}$マウスにおいてAIMを欠損させると動脈硬化の進行が著しく抑制された．このことは，大動脈弁部だけでなく，腹部大動脈でも観察された．（文献6より）

されていることから[7]，LXR以外の発現誘導機構の存在，そしてある特定の環境下ではマクロファージ以外にもAIMを発現する細胞が存在する可能性が示唆される．

Ⅱ．AIMと動脈硬化

1．動脈硬化の病態生理

動脈硬化は国内外で最も高い死因の一つとなっているメタボリック症候群の中心的疾患である．血液中のコレステロール値が上昇すると，動脈の血管内皮下層で酸化されたLDL（low density lipoprotein）が血管内皮細胞を刺激することによって様々な接着因子やケモカインを産生し，それが血中内を循環する単球を呼び寄せる．内皮下層に浸潤した単球はマクロファージへと分化し，SR-AやCD36といったスカベンジャー受容体を介して酸化LDLを取り込む．酸化LDLは分解されてコレステロールエステルとして細胞内に蓄積され，マクロファージは次第に肥大化して脂肪滴を泡のように含んだ泡沫化細胞となる．このような泡沫化マクロファージが血管内皮下層に蓄積すると，それらの産生するサイトカイン類や炎症反応の影響で血管平滑筋層からの平滑筋細胞の遊走・増殖，そして泡沫化が起こり，やがてコラーゲンなどの細胞外マトリクスが分泌されていわゆる線維性プラークを形成する（図1）[8]．

この過程において，病巣における炎症反応は病状を悪化させる重要なファクターである．硬化巣に浸潤し

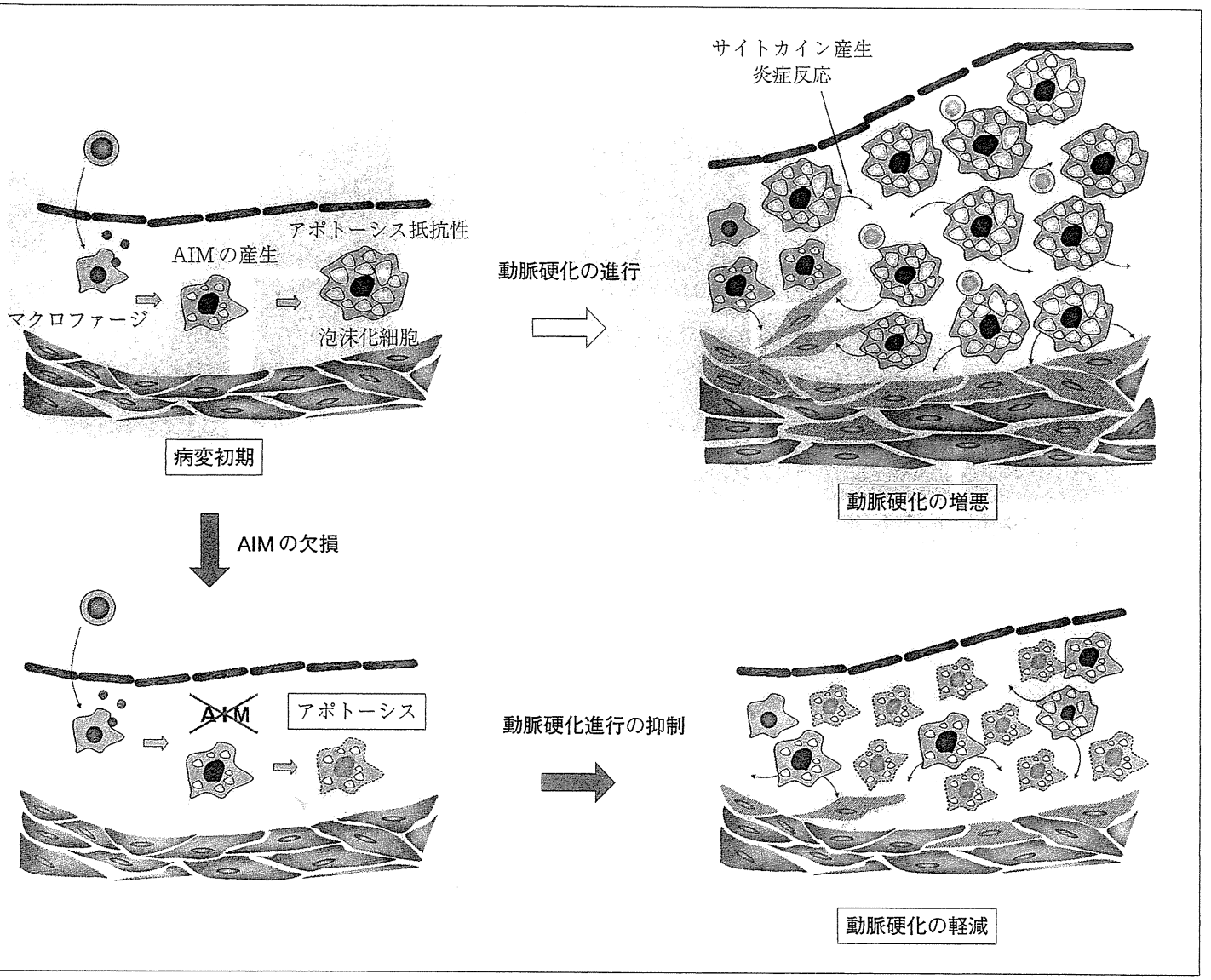

図3　動脈硬化におけるAIMの役割　AIMを欠損することで硬化巣マクロファージにアポトーシスを誘導することにより，泡沫化マクロファージの蓄積を妨げ，また炎症反応を抑制することで病態の進行が軽減される．（文献6より）

たT細胞は病巣マクロファージと相互作用し，炎症反応を誘起する．また，TNFα（tumor necrosis factor α）やIL-6（interleukin-6）といった炎症性サイトカインが持続的に産生され，炎症反応がやがて慢性的になるとこれらの悪循環により病態進行が加速度的に増すこととなる[8]．

2．動脈硬化における細胞死

動脈硬化巣組織はアポトーシスを誘引するファクターに満ちている．例えば，酸化LDLやその分解物であるオキシステロールoxysterol，TNFα，Fas-Fasリガンド系等の細胞間相互作用，一酸化窒素（NO）などである．さらに，局所的な低栄養状態，低酸素状態等の環境悪化もアポトーシス誘導の原因となりうる[9]．また，細胞の泡沫化，すなわちエステル化されていないコレステロール（free cholesterol：FC）の細胞内蓄積も細胞にとっては好ましくない．特に，進行した動脈硬化においては，細胞内におけるFCの過剰な蓄積が細胞死の大きな原因となる[10]．

近年，動脈硬化巣マクロファージのアポトーシスは病態進行を軽減するという考えが一般的になりつつある．硬化巣マクロファージがアポトーシスを起こすと，蓄積する細胞数が減少するだけでなく，病巣における炎症反応の抑制にもつながる．アポトーシス細胞を貪食することにより，マクロファージの炎症シグナルの抑制と抗炎症シグナルの活性化が起こるとも報告されている[11]．しかしながら，実際は先述のような劣悪な環境化に置かれながらも硬化巣マクロファージはアポトーシスに対し抵抗性を示すことでプラークの肥

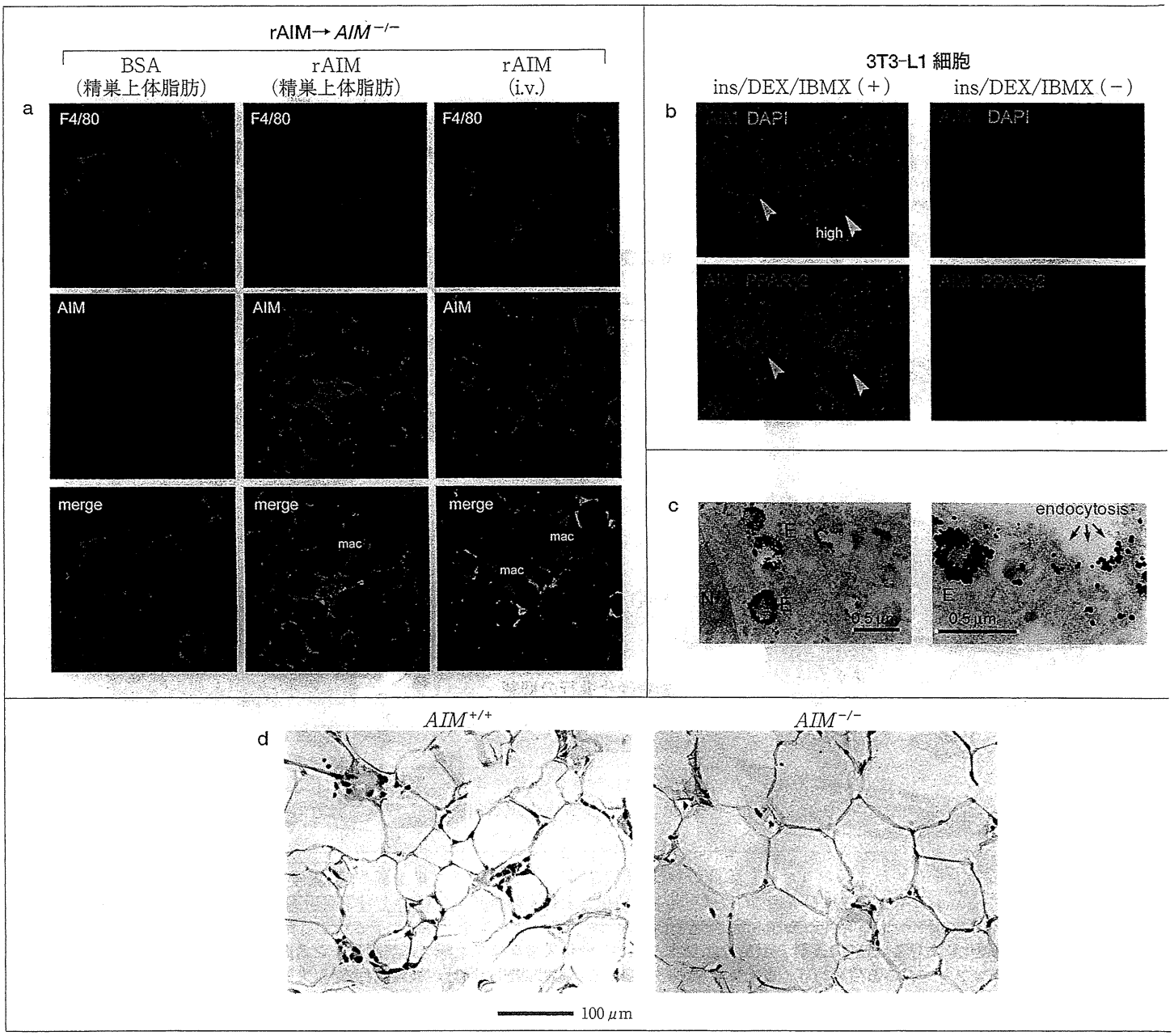

図4　脂肪細胞とAIM　a：肥満脂肪組織によるAIMの取り込み．肥満を誘導した*AIM*$^{-/-}$マウスにおいて，精巣上体脂肪に直接（真中），および尾静脈注射（右）により組換型AIM（rAIM）を注入し，3時間後に精巣上体脂肪を取り出して固定し，マクロファージ（F4/80，赤），AIM（緑）について各抗体を用いて染色した．rAIMを注入した組織では，脂肪細胞の細胞質においてAIMのシグナルが確認され，AIMが脂肪細胞に取り込まれていることがわかる．なお，マクロファージもAIMを取り込んでいる．mac：マクロファージ．b：3T3-L1脂肪細胞によるAIMの取り込み．インスリン（ins），dexamethasone（DEX），isobutyl methylxanthine（IBMX）により刺激し，脂肪細胞へ分化させた3T3-L1脂肪細胞にrAIMを添加し，3時間後に抗AIM抗体を用いて免疫細胞化学染色を行った（AIM，赤）．同時にPPARγ2（緑）についても染色を行った．黄色矢頭で示したようにPPARγ2を高発現している細胞（high）においてAIMの取り込みがみられる．一方，分化刺激を加えていない未分化の細胞（右）はAIMを取り込まない．c：3T3-L1脂肪細胞によるAIMの取り込み（免疫電子顕微鏡）．bと同様に分化させた3T3-L1脂肪細胞にrAIMを添加し，抗AIM抗体を用いて免疫電子顕微鏡にて解析した．取り込まれたAIM（黒いドット）がエンドソームの膜状に集積しているのがわかる．E：endosome，N：nucleus．d：*AIM*$^{+/+}$および*AIM*$^{-/-}$マウスの肥満脂肪組織．高脂肪食を20週間負荷して肥満化させた*AIM*$^{+/+}$および*AIM*$^{-/-}$マウスの精巣上体脂肪組織のHE染色．*AIM*$^{-/-}$マウスの脂肪細胞の大きさが大きいことがわかる．（文献5より）

厚と慢性炎症の原因となっている．このアポトーシス抵抗性の原因の一つにアポトーシス抑制因子AIMが挙げられる．

3. AIMと動脈硬化

先述のように，動脈硬化巣に蓄積する泡沫化マクロファージは酸化LDLの刺激によりLXRが活性化して

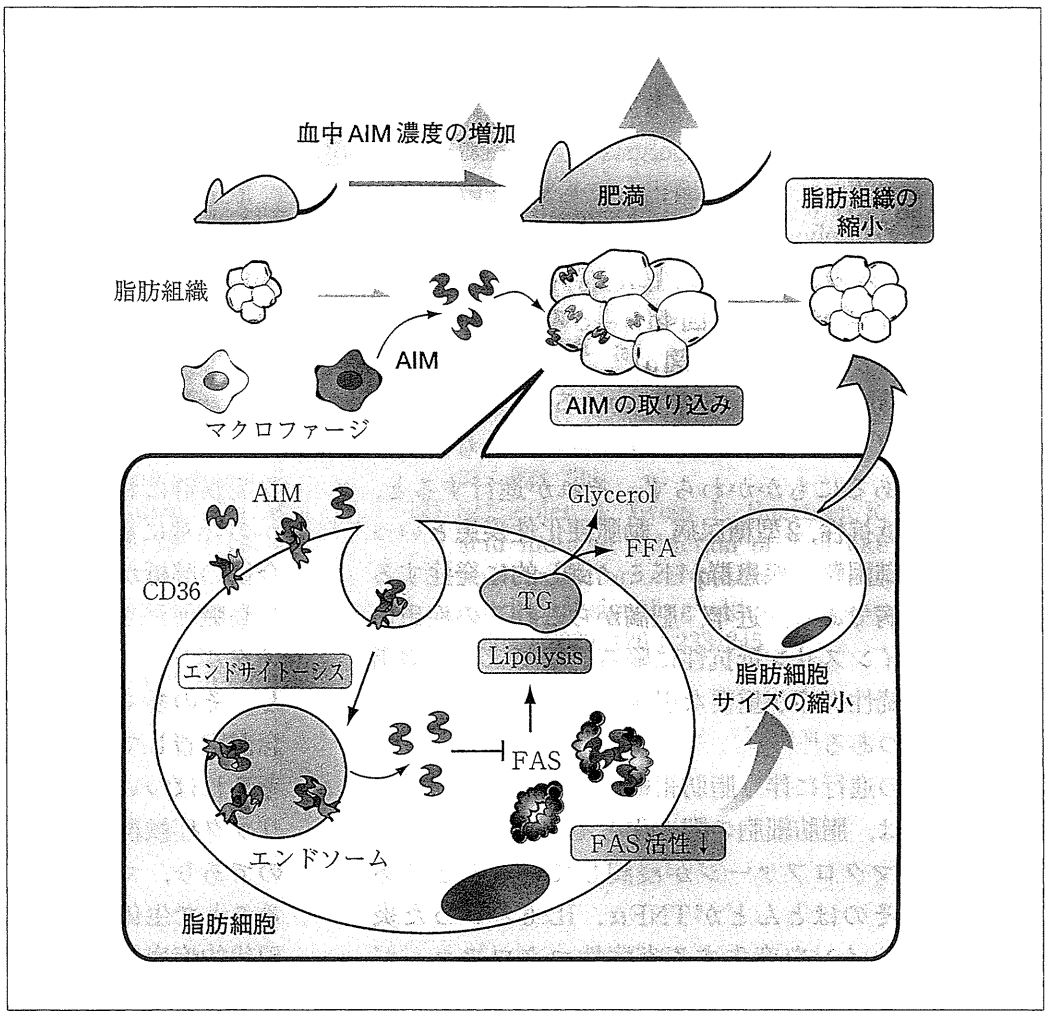

図5　肥満の進行と脂肪細胞によるAIMの取り込み（まとめ）　肥満が進行するとAIMの血中濃度が上昇することで，脂肪組織によるAIMの取り込みが起こる．AIMは脂肪細胞内でFASに結合することでその活性を阻害し，lipolysisを誘導するため，FFAが放出される．このように，貯蔵されていたTG（triglyceride）が分解されるため，脂肪細胞のサイズは小さくなり，それに伴い脂肪組織も縮小する．（文献5より）

おり，AIMを非常に強く発現している．このことは，動脈硬化モデルマウスである*LDLR*$^{-/-}$マウス（LDL receptorノックアウトマウス：血中のLDL濃度が上昇するため，高コレステロール食負荷により動脈硬化症を発症する）（**図2a**），およびヒト患者の動脈硬化巣において確認された[6]．すなわち，硬化巣に蓄積するマクロファージはAIMを強く発現しているために容易にアポトーシスに陥らず，病態悪化の原因になっているといえる．実際に，AIMを欠損した動脈硬化モデルマウス（*AIM*$^{-/-}$*LDLR*$^{-/-}$マウス）では，硬化巣においてマクロファージのアポトーシスの顕著な増加がみられ，さらにそれに伴う病巣の炎症反応の軽減により，病態の初期から後期にかけて動脈硬化の著しい軽減が観察された（**図2b**）．このように，AIMは硬化巣マクロファージにアポトーシス抵抗性をもたらし，病態進行に深く関与していることが示された（**図3**）[6]．

Ⅲ．AIMと脂肪細胞

1．AIMのlipolysis機能

これまで我々は主にマクロファージに対するAIMのアポトーシス抑制機能に着目して研究を行ってきたが，最近，AIMの新たな標的細胞とそれにおける新しい機能を発見し，AIMが動脈硬化に限らずメタボリック症候群に非常に深く関与していることを見出した．その発見は以下のようなものである[5]．

（1）AIMは脂肪細胞によってCD36を介してエンドサイトーシスにより取り込まれる（**図4a～c**）．

（2）AIMは細胞内でエンドソームからリリースされると細胞質中の脂肪酸合成酵素fatty acid synthase（FAS）に結合することでその酵素活性を抑制する．

（3）その結果，脂肪細胞において貯蔵していたlipolysisを誘導し，遊離脂肪酸free fatty acid（FFA）が放出される．

分泌型蛋白質であるAIMは通常も血中に存在する

が(マウスで約10 mg/L程度)，肥満の進行に伴い血中濃度が急激に上昇する(マウスでは約5倍～)．そのため，肥満化した生体における脂肪組織ではAIMをより取り込むようになり，lipolysisが誘導される．逆に*AIM*$^{-/-}$マウスでは，肥満化してもAIMの取り込みがないためlipolysisも抑えられる．その結果，肥満*AIM*$^{-/-}$マウスの脂肪細胞は*AIM*$^{+/+}$マウスのそれと比較してサイズが大きく(**図4d**)，そのため内臓脂肪の量も多いことがわかった(**図5**)[5]．

2．肥満脂肪組織の慢性炎症におけるAIMの役割

周知のとおり，メタボリック症候群は，入り口は単なる肥満であるにもかかわらず，それが進行すると，インスリン抵抗性，2型糖尿病，動脈硬化性疾患といった様々な制御困難な疾患群がドミノ倒し的に発症する深刻な現代病である．近年，肥満からこれらの疾患の根幹を成すインスリン抵抗性に陥る過程では，内臓脂肪の慢性持続性炎症が重要な引き金となることが明らかになりつつある[12,13]．

この肥満の進行に伴う脂肪組織の炎症性変化の最も特徴的な点は，脂肪細胞の肥大化とその数の増加と同時に多数のマクロファージが浸潤していることである．そしてそのほとんどがTNFα，IL-6といった炎症性サイトカインを産生する炎症性マクロファージ(M1マクロファージ)であり，肥大化した脂肪細胞とクロストークすることで慢性的に炎症が持続する．この炎症性変化の初期には脂肪細胞からのケモカイン産生が増大することで，マクロファージの浸潤が誘導されると考えられているが，詳細は明らかになっていない．

マクロファージ浸潤の原因となるケモカイン産生を誘導する因子には様々な要因が考えられるが，最近，パルミチン酸等の飽和脂肪酸が脂肪細胞に発現するTLR4(Toll-like receptor 4)の内因性リガンドとして作用し，その結果ケモカインであるMCP-1(monocyte chemotactic protein-1)の発現を誘導することが報告されている[14]．先に述べたように，肥満の進行に伴いAIMの血中濃度が上昇することで脂肪細胞がそれを取り込みlipolysisが誘導されるが，そこで放出されるFFAにより局所的にTLR4が刺激され，ケモカイン産生が誘導される可能性が示唆される．この「肥満脂肪細胞によるAIMの取り込み→lipolysis→マクロファージ浸潤」のシークエンシャルなプロセスについては現在解析中であるが，もしこの図式が成り立てば，肥満から起こるメタボリック症候群の疾患連鎖のその初期においてAIMが非常に重要な役割を果たしている可能性が示唆される．

おわりに

最近，メタボリック症候群におけるAIMの重要が次々に明らかになりつつある．動脈硬化において硬化巣の泡沫化マクロファージにアポトーシス抵抗をもたらせることで病態を悪化させ，肥満脂肪組織においてはlipolysisを誘導することで脂肪細胞を縮小せる．しかしながら後者はlipolysisにより脂肪組織マクロファージ浸潤を誘起させることで，メタボリック症候群における肥満からその先の疾患へ進むかどかの非常に重要なプロセスに関与する可能性があり今後の解析が待たれるところである．

動脈硬化や肥満脂肪組織の慢性炎症を含めた多くメタボリック症候群においてマクロファージが関し，その多くが病態を悪化させる方向へ働くという念が定着してきたのはこれまでの医学研究の歴史か考えればつい最近のことと思われる．すなわちメタリック症候群という疾患そのものが非常に現代的なのであり，マクロファージという本来は異物を排除ることで生体を防御する性質をもつはずのものがこ現代的疾患では行き過ぎたものになってしまうと解できるだろう．そのような流れの中で，AIMとい分子もこのそれぞれの病態に負の方向に関与してい点は非常に興味深い．メタボリック症候群のよう「正常な生理作用の蓄積による疾患」をいかに食いめるかを考えるときは，このような分子に着目するとで新しい予防・治療への道が開けるかもしれない今後の新しい創薬ターゲットとしての可能性を含め我々のAIMに対する興味は尽きるところがない．

文　献

1) Miyazaki, T., Hirokami, Y., Matsuhashi, N. et al. Increased susceptibility of thymocytes to apoptsis in mice lacking AIM, a novel murine macrphage-derived soluble factor belonging to th scavenger receptor cysteine-rich domain supefamily. J Exp Med 1999, **189**：413-422
2) Maxwell, K.N., Soccio, R.E., Duncan, E.M. et al. Novel putative SREBP and LXR target gene identified by microarray analysis in liver of chlesterol-fed mice. J Lipid Res 2003, **44**：2109-211
3) Kuwata, K., Watanabe, H., Jiang, S.Y. et al.：AI inhibits apoptosis of T cells and NKT cells in C rynebacterium-induced granuloma formation mice. Am J Pathol 2003, **162**：837-847
4) Joseph, S.B., Castrillo, A., Laffitte, B.A. et al.：R